

# Heat flux and Flow topology statistics in oblique quenching of turbulent premixed flames by isothermal inert walls

Jiawei Lai, Nilanjan Chakraborty  
 School of Mechanical Engineering, Newcastle University  
 Newcastle-Upon-Tyne, Tyne and Wear, NE1 7U, United Kingdom

## 1 Introduction

Direct Numerical Simulations (DNS) have contributed significantly to the fundamental understanding and modelling of turbulent fluid flows in last two decades. However, to date, relatively limited effort has been directed to DNS of flame-wall interaction. The nature of dominant flow topologies in the case of flame-wall interaction and their relative contributions to wall heat flux are yet to be analysed in detail. This gap in existing literature has been addressed here by carrying out 3D compressible DNS simulations of turbulent V-flame with isothermal inert walls. The flame holder is kept closer to one of the walls (here the bottom wall) for the purpose of inducing flame-wall interaction. A similar configuration was used in the past by Alshaalan and Rutland [1]. Here, the flow topologies have been characterised with the help of three invariants (i.e. first– $P$ , second– $Q$  and third– $R$ ) of the velocity gradient  $\partial u_i / \partial x_j$  tensor following Chong *et al.* [2]. Based on the statistical behaviors of  $P$ ,  $Q$  and  $R$ , the flow topologies can be categorised into 8 categories (i.e. S1-S8), as shown in Fig. 1. The evolution of flow topologies in the near-wall region with the progress of flame quenching has been analysed here in detail. Moreover, their contributions to wall heat flux have been identified and physical explanations have been provided for the observed findings. Furthermore, the wall heat flux and flame quenching distance statistics for oblique flame-wall interaction in the case of a turbulent V-flame have been compared to the corresponding values obtained for the Head-on Quenching (HOQ) configuration for statistically planar turbulent premixed flames.

## 2 Mathematical Background and Numerical Implementation

The local flow topologies are characterised here by the invariants of the velocity-gradient tensor [2]:  $A_{ij} = \partial u_i / \partial x_j = S_{ij} + W_{ij}$  where the symmetric strain-rate tensor is  $S_{ij} = 0.5(A_{ij} + A_{ji})$  and the anti-symmetric rotation rate tensor is  $W_{ij} = 0.5(A_{ij} - A_{ji})$ . The eigenvalues of  $A_{ij}$  are  $\lambda_1, \lambda_2$  and  $\lambda_3$  which are the solutions of the characteristics equation  $\lambda^3 + P\lambda^2 + Q\lambda + R = 0$  with its invariants  $P, Q$  and  $R$  as specified below [2]:

$$P = -tr(A_{ij}) = -(\lambda_1 + \lambda_2 + \lambda_3) = -S_{ii} \quad (1)$$

$$Q = 0.5([\text{tr}(A_{ij})]^2 - \text{tr}(A_{ij}^2)) = 0.5(P^2 - S_{ij}S_{ij} + W_{ij}W_{ij}) = Q_S + \underbrace{W_{ij}W_{ij}/2}_{Q_W} \quad (2)$$

$$R = -\det(A_{ij}) = (-P^3 + 3PQ - S_{ij}S_{jk}S_{ki} - 3W_{ij}W_{jk}S_{ki})/3 \quad (3)$$

The discriminant  $D$ , is shown in the equation below, divides the  $P - Q - R$  phase space into two regions:  $A_{ij}$  shows a focal topology for  $D > 0$  and it displays a nodal topology for  $D < 0$  [2]:

$$D = [27R^2 + (4P^3 - 18PQ)R + 4Q^3 - P^2Q^2]/108 \quad (4)$$

The surface  $D = 0$  leads to two surfaces  $r_{1a}$  and  $r_{1b}$  in the  $P - Q - R$  phase space:

$$r_{1a} = P(Q - 2P^2/9)/3 - 2(-3Q + P^2)^{3/2}/27 \quad (5)$$

$$r_{1b} = P(Q - 2P^2/9)/3 + 2(-3Q + P^2)^{3/2}/27 \quad (6)$$

Additionally,  $A_{ij}$  has purely imaginary eigenvalues on the surface  $r_2$  which is given by  $R = PQ$ . The surface  $r_{1a}$ ,  $r_{1b}$  and  $r_2$ , where  $r_2$  is described by  $PQ - R = 0$ , divide the  $P - Q - R$  phase space into the 8 flow topologies as shown in Fig. 1.

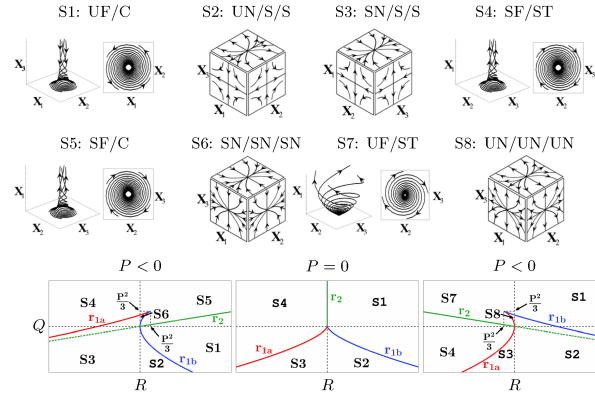


Figure 1: Classification of S1-S8 topologies (UF = unstable focus, UN = unstable node, SF = stable focus, SN = stable node, S = saddle, C = compressing, ST = stretching) in the  $Q - R$  plane with the lines  $r_{1a}$ ,  $r_{1b}$  and  $r_2$  dividing the topologies, and black dark line indicates  $Q = 0$  and  $R = 0$ .

A well-known three-dimensional compressible DNS code SENGAs [3] has been used to simulate the oblique quenching of a V-flame by two isothermal inert sidewalls as shown in Fig. 2. A single step irreversible chemistry (i.e.  $Fuel + s Oxidiser \rightarrow (1+s) Products$ ) is used for the purpose of computational economy. The simulation domain is taken to be a rectangular box of size  $175.8\delta_Z \times 58.5\delta_Z \times 58.5\delta_Z$  (where the long-side of the domain is aligned with  $x_1$ -direction) where  $\delta_Z = \alpha_{T0}/S_L$  is the Zel'dovich thickness with  $\alpha_{T0}$  and  $S_L$  being the thermal diffusivity of the unburned gas and the unstrained laminar burning velocity respectively. The computational domain is discretised by a uniform Cartesian mesh of size  $900 \times 300 \times 300$ , ensuring at least 10 grid points across the thermal flame thickness  $\delta_{th} = (T_{ad} - T_0)/\max|\nabla \hat{T}|_L$ , where  $T_{ad}$ ,  $T_0$  and  $\hat{T}$  are the adiabatic, unburned and instantaneous temperature respectively, and the sub-script  $L$  denotes the steady unstrained planar flame values. Furthermore, this resolution ensures that normalised grid size  $\rho_0 u_\tau \Delta x / \mu_0$  remains smaller than unity, where  $u_\tau$ ,  $\rho_0$  and  $\mu_0$  are the friction velocity, unburned gas density and unburned gas viscosity, respectively. No-slip isothermal inert walls with temperature  $T_W = T_0$ , with zero wall-normal mass flux is specified at  $x_2 = 0$  (for bottom wall) and  $x_2 = L_2$  (for upper wall where  $L_2$  is the domain length in  $x_2$ -direction). Turbulent inflow with specified velocity components and density at  $x_1 = 0$ , and partially non-reflecting boundary for the face opposite to the turbulent inlet are used as boundary conditions. The boundaries in the  $x_3$ -direction are taken to be periodic. A plane is

scanned through a frozen field of turbulent velocity fluctuations, and the Taylor's hypothesis is used for specifying inlet turbulent velocity fluctuations. A flame holder with a radius of  $R_{fh} \approx 1.5\delta_{th}$  is placed at a distance  $44\delta_Z$  from the inlet and  $14.6\delta_Z$  from the bottom wall to ensure the flame interacts more readily with the bottom wall. At the flame holder, the species, temperature and velocity distributions were imposed using a presumed Gaussian function following Dunstan *et al.* [4]. The formation of boundary layer on the flame holder and the effects of shear generated turbulence due to the flame holder are not considered in this analysis. The inlet values of normalised root-mean-square turbulent velocity  $u'/S_L$  and normalised integral length scale  $l/\delta_{th}$  are taken to be 5.0 and 1.67 respectively, and the corresponding values of  $Da$  and  $Ka$  are given by 0.33 and 8.65 respectively for the V-flame case. The mean inlet velocity  $U_{mean}$  is taken to be  $12.0S_L$  for the V-flame simulation. The V-flame simulation has been carried out for more than two complete flow-through times (i.e.  $2.39t_{ft} = 2.39L_1/U_{mean}$ , where  $L_1$  is the domain length in  $x_1$ -direction). Standard values are considered for the Zel'dovich number  $\beta = T_{ac}(T_{ad} - T_0)/T_{ad}^2$  and the ratio of specific heats (i.e.  $\beta = 6.0$  and  $\gamma = 1.4$ ), where  $T_{ac}$  is the activation temperature. The oxidiser to fuel ratio by mass  $s$ , heat release parameter  $\tau = (T_{ad} - T_0)/T_0$  and equivalence ratio  $\phi$  are taken to be 4.0, 2.3 and 1.0 respectively. The Lewis number  $Le$  of all the species are taken to be unity for all cases considered here. The value of  $s = 4.0$  is representative of methane-air combustion. High order finite-difference and Runge-Kutta schemes are used for spatial discretisation and explicit time-marching respectively.

A HOQ configuration for a statistically planar premixed flame has also been considered which has the same thermo-chemistry and numerical methodology as that of the V-flame case in order to compare the statistics of wall heat flux, quenching distance and flow topology distributions. The simulation domain for the HOQ case is taken to be  $70.6\delta_Z \times 35.2\delta_Z \times 35.2\delta_Z$  which is discretised by uniform Cartesian mesh of size  $512 \times 256 \times 256$ . Moreover, the initial values of  $u'/S_L$  and  $l/\delta_{th}$  are taken to be 5.0 and 1.67 respectively. In HOQ configuration, an isothermal inert non-slip wall with  $T_W = T_0$  is specified at  $x_1 = 0$ , and the mass flux is specified to be zero in the wall normal direction. The boundary opposite to the wall is taken to be partially non-reflecting, whereas the transverse boundaries are taken to be periodic. Initially the isosurface corresponding to  $(\hat{T} - T_0)/(T_{ad} - T_0) = 0.9$  is kept  $20\delta_Z$  away from the wall and the HOQ simulation has been continued until the maximum and minimum value of wall heat flux assume same values following the flame quenching, and this time corresponds to  $t \approx 22\delta_Z/S_L$  for the case considered here.

### 3 Results & Discussion

The instantaneous distribution of vorticity magnitude (i.e.  $\sqrt{\omega_i\omega_i}$  with  $\omega_i$  being the  $i^{\text{th}}$  component of vorticity) is shown in Fig. 2a which shows the magnitude of  $\sqrt{\omega_i\omega_i}$  decreases significantly across the flame. The instantaneous distributions of non-dimensional temperature (i.e.  $T = (\hat{T} - T_0)/(T_{ad} - T_0)$ ) on the  $x_1 - x_2$  side plane and fuel mass fraction  $Y_F$  on the bottom wall surface are also shown in Fig. 2a. The flame quenches due to heat loss through the wall which leads to diffusion of remaining fuel from the near-wall region to the gaseous mixture at the interior of the domain and thus the magnitude of fuel mass fraction  $Y_F$  drops in the region where the flame interacts with the wall. For the present analysis, the reaction progress variable  $c$  is defined in terms of the fuel mass fraction  $Y_F$  as:  $c = (Y_{F0} - Y_F)/(Y_{F0} - Y_{F\infty})$  where the subscripts 0 and  $\infty$  denote the values in the unburned gas and fully burned products, respectively. The contours of  $T$  and  $c$  are shown for the  $x_1 - x_2$  mid-plane in Fig. 2b. A careful comparison between  $c$  and  $T$  reveals that  $c = T$  where the flame is away from the wall. However, an inequality between the reaction progress variable and non-dimensional temperature (i.e.  $c \neq T$ ) is obtained in the vicinity of the wall. The difference in boundary condition (i.e. Dirichlet boundary condition for temperature and Neumann boundary condition for species mass fractions) leads to an inequality between  $c$  and  $T$ .

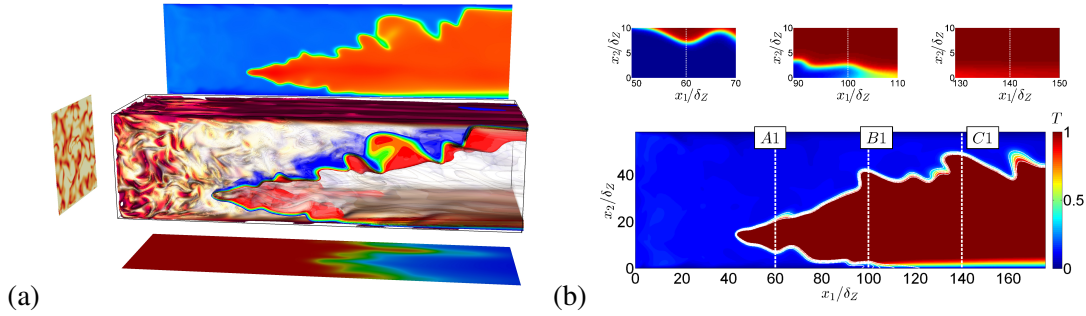


Figure 2: (a) The instantaneous distribution of vorticity magnitude (background: red-high and white-low) and non-dimensional temperature (isosurface and side view, red-high and blue-low) and fuel mass fraction (lower wall view, red-high and blue-low) for the V-flame case. (b) Distributions of  $T$  and  $c$  (shown by white lines from 0 to 1 with 0.2 interval) at  $t = 2t_{ft}$  for  $x_1 - x_2$  mid-plane. Distributions of  $c$  around locations A1, B1 and C1 are shown in the inset. The locations A1, B1 and C1 in Fig. 2b correspond to  $x_1 = 60\delta_Z$ ,  $100\delta_Z$  and  $140\delta_Z$  respectively.

The temporal evolutions of non-dimensional wall heat flux magnitude  $\Phi = |q_w|/[\rho_0 C_P S_L (T_{ad} - T_0)]$  and Peclet number  $Pe = X/\delta_Z$  for top and bottom walls for the V-flame case are shown in Fig. 3, where  $X$  is the wall normal distance of the nearest  $T = 0.9$  isosurface [3,5] and  $q_w = -\lambda(\partial\hat{T}/\partial n)_w$  is the wall heat flux with  $C_P$ ,  $\lambda$  and  $n$  being the specific heat at constant pressure, thermal conductivity and wall normal direction respectively. The corresponding temporal variations of  $\Phi$  and Peclet number  $Pe$  for HOQ of a statistically planar flame with initial values of  $u'/S_L$  and  $l/\delta_{th}$  equal to the inlet values for the turbulent V-flame case are also shown in Fig. 3. The Peclet number for HOQ drops with time as the flame advances towards the wall. The mean value of  $\Phi$  increases as the mean Peclet number  $Pe$  decreases with time. The maximum value of normalised wall heat flux  $\Phi_{max}$  in the case of HOQ is obtained at a time when the minimum Peclet number  $Pe_{min}$  is attained. The values of  $\Phi_{max}$  and  $Pe_{min}$  for laminar HOQ are given by 0.39 and 2.53 respectively. These values are consistent with previous experimental [6,7] and computational [3,5]. The magnitude of  $|q_w|$  can be scaled as:  $|q_w| \sim \lambda(T_{ad} - T_0)/X$ , which leads to  $\Phi \sim 1/Pe$  and accordingly one obtains the following relation:  $\Phi_{max} \sim 1/Pe_{min}$ . For turbulent HOQ one obtains  $\Phi_{max} = 0.42$  and  $Pe_{min} = 2.16$  which suggest that the maximum heat flux and the minimum Peclet number values in turbulent HOQ remain almost equal to the corresponding values for laminar HOQ. By contrast,  $Pe_{min}$  for the turbulent V-flame case is found to be 1.71 whereas  $\Phi_{max}$  assumes a value of 0.63. According to the scaling  $\Phi_{max} \sim 1/Pe_{min}$ , a smaller value of  $Pe_{min}$  in the turbulent V-flame case than in the HOQ of statistically planar flame leads to a higher value of normalised wall heat flux  $\Phi_{max}$  in the turbulent V-flame case. It can be seen from Fig. 3 that  $Pe$  values are higher for the top wall than for the bottom wall because the flame holder is placed closer to the bottom wall so that the flame-wall interaction takes place more readily for the bottom wall. For the turbulent HOQ case, the maximum value of Peclet number increases initially with time due to flame wrinkles which are concavely curved towards the reactants. As the flame advances towards the wall the maximum, mean and minimum values of Peclet number decrease until flame quenching. The decreases of the maximum, mean and minimum values of Peclet number are associated with the increases in minimum, mean and maximum values of  $\Phi$  with time. After flame quenching the isotherms move away from the wall [3] in the HOQ configuration. By contrast, the Peclet number  $Pe$  does not change much following flame quenching in the V-flame configuration. In the case of oblique flame quenching, the fluid velocity remains small in the near-wall region, and thus the flame can reach closer to the wall before quenching than in the corresponding HOQ case. It can be seen from Fig. 3 that the maximum normalised heat flux  $\Phi_{max}$  for both top and bottom walls remain comparable but  $\Phi_{max}$  for the bottom wall attains higher value than the value obtained for the top wall. The smaller values of the minimum Peclet number

for the bottom wall are reflected in the higher value of  $\Phi_{max}$  than in the case of the top wall. Moreover, the mean heat flux is greater for the bottom wall than that for the top wall because the flame remains closer to the bottom wall. It can further be seen from Fig. 3 that the extent of the fluctuation of  $\Phi_{max}$  for the top wall is greater than the bottom wall. The wall heat flux rises sharply when the turbulent fluid motion brings the flame elements close to the wall and similarly heat flux drops when either the flame quenches or the flame moves away from the wall under the influence of turbulence. Since the bottom wall remains closer to the flame it interacts more readily than the top wall, which leads to less rapid changes in the  $\Phi_{max}$  for the bottom wall.

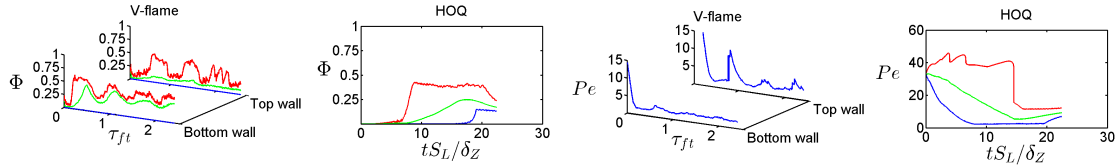


Figure 3: Variations of  $\Phi$  and  $Pe$  (maximum (—); mean (—); minimum (—)).

In order to understand the flow contribution to the wall heat flux, the distributions of the volume fractions  $VF$  of the flow topologies conditional on reaction progress variable  $c$  at locations A1, B1 and C1 are shown in Fig. 4 for  $t = 2.39t_{ft}$  but the qualitative nature of the distribution remains unchanged since  $t = 1.0t_{ft}$ . It is worth noting that the flame does not interact with the wall at location A1 where the volume fractions of S2 and S7 topologies are the leading contributors within the flame front. This is consistent with the topology variation in the corresponding turbulent HOQ case. The topologies which are typical of negative dilatation rate (i.e. S5 and S6) are rare at location A1 but the volume fraction of S5 topology assumes non-negligible value at locations B1 and C1. A similar increase of  $VF$  of S5 and S6 topologies can be observed at later times in the turbulent HOQ case during advanced stage of quenching (i.e.  $t = 20\delta_Z/S_L$ ). A comparison between locations A1, B1 and C1 reveals that the flame-wall interaction and flow development in the downstream of the flame holder significantly affect the distribution of flow topologies. The relative contribution of the S7 topology decreases from A1 to C1, whereas the relative contribution of S8 topology increases in the downstream and it becomes a dominant contributor at location C1. A qualitatively similar transition in behaviour can also be observed in the turbulent HOQ case, as the quenching progresses with time. The S2 topology remains a dominant contributor and the contributions of S1, S3 and S4 remain significant at all locations (times) for the V-flame case (HOQ case).

The percentages of wall heat flux magnitude contribution by individual flow topologies for the V-flame and HOQ cases are shown in Fig. 5 at different time instants. Figure 5 shows that the S1 and S4 topologies contribute significantly to heat flux for both walls in the V-flame case. However, the S1 topology is the leading contributor for the bottom wall, whereas the S4 topology is the leading contributor for the top wall in the V-flame case. It can be seen from Fig. 4 that  $VF$  values for the S1 and S4 topologies increase in the unburned and burned gas regions ( $c = 0$  and  $c = 1$ ). As either unburned or burned gases are predominantly found at the wall, the topologies S1 and S4 contribute significantly to the wall heat flux. Moreover, the shear rate introduced by the walls generate vorticity in the near-wall region and thus the focal topologies S1 and S4 contribute to wall heat flux in the V-flame case. A comparison between Figs. 3 and 5 for the HOQ case reveals that all topologies except S5 and S6 have comparable wall heat flux contributions when the flame begins to interact with the wall. The nodal topologies S2 and S3 become the major contributors to the wall heat flux when  $\Phi_{max}$  attains its peak value. The contributions of all flow topologies to the wall heat flux become comparable when the maximum, mean and minimum values of  $\Phi$  approach each other but the contributions of the S1, S3-S8 topologies remain greater than the S2 topology.

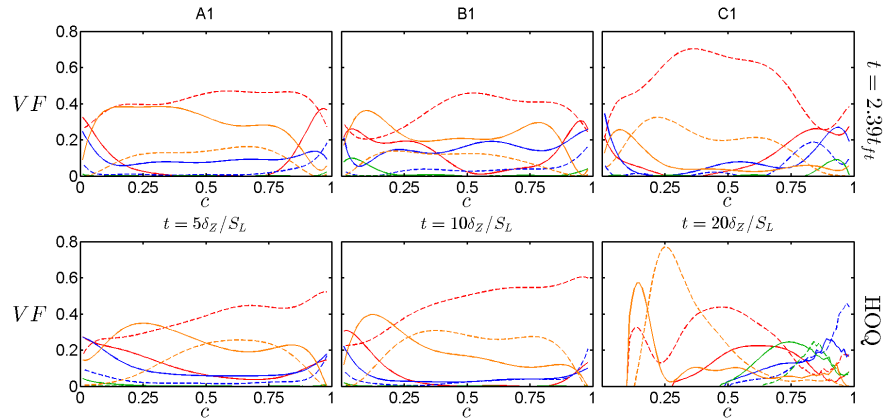


Figure 4: Variations of volume fraction  $VF$  for topologies conditional on  $c$ . Top figures: locations A1, B1 and C1 in the V-flame case at  $t = 2.39t_{ft}$ ; Bottom figures: for the HOQ case at three time instants. Focal topologies S1 (—), S4 (—), S5 (—), S7 (—), nodal topologies S2 (---), S3 (---), S6 (---), S8 (---).

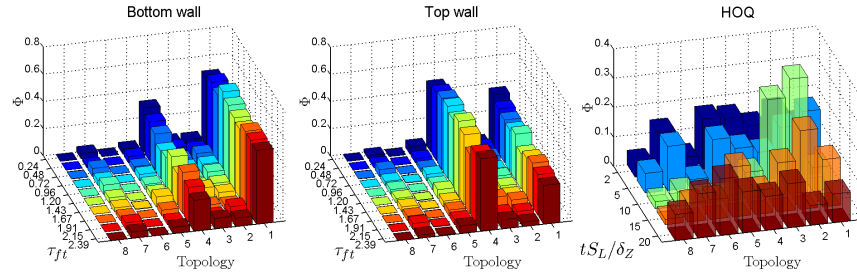


Figure 5: Percentages of wall heat flux magnitude contributions arising from individual flow topologies S1-S8 in the V-flame case from  $0.24t_{ft}$  to  $2.39t_{ft}$  (1<sup>st</sup> -2<sup>nd</sup> column) and HOQ case from  $t = 2\delta z/S_L$  to  $20\delta z/S_L$  (3<sup>rd</sup> column).

## 4 Conclusions

The statistics of wall heat flux, flame quenching distance in the case of oblique quenching of a turbulent V-flame by isothermal inert walls have been analysed in terms of the distributions of flow topologies and their contributions using DNS data. It has been found that the maximum (minimum) wall heat flux (Peclet number) in the case of oblique flame quenching assumes greater (smaller) value than in the corresponding turbulent HOQ case. Although the volume fractions of S2 and S7 topologies assume high values within the flame front, the focal topologies S1 and S4 have been found to be the significant contributors to the wall heat flux in the case oblique flame quenching. By contrast, nodal topologies S2 and S3 remain major contributors to the wall heat flux when it attains large magnitude in the HOQ case but all topologies contribute comparably to the wall heat flux at later stages of flame quenching.

## References

- [1] Alshaalaa, T.M., Rutland, C.J. (1998) Proc. Combust. Inst. 27:793.
- [2] Chong, M., Perry, A. and Cantwell, B. (1990) Phys. Fluids. 2:765.
- [3] Lai, J., Chakraborty, N. (2016) Flow, Turb. Combust. 96:279.
- [4] Dunstan, T.D., Swaminathan, N., Bray, K.N.C., Cant, R.S. (2011) Flow Turb. Combust., 87: 725.
- [5] Poinso, T., Haworth, D., Bruneaux, G. (1993) Combust. Flame. 95:118.
- [6] Huang, W.M., Vosen, S.R. and Greif, R. (1986) Proc. Combust. Inst., 21: 1853.
- [7] Jarosinsky, J. (1986) Combust. Sci. Technol. 12:81.